MATERIALS SCIENCE

Effect of structure: A new insight into nanoparticle assemblies from inanimate to animate

Chuanhui Huang[1]*, Xiangyu Chen[1]*, Zhenjie Xue[1,2], Tie Wang[1,2†]

Copyright © 2020 The Authors, some rights reserved; exclusive licensee American Association for the Advancement of Science. No claim to original U.S. Government Works. Distributed under a Creative Commons Attribution NonCommercial License 4.0 (CC BY-NC).

Nanoparticle (NP) assemblies are among the foremost achievements of nanoscience and nanotechnology because their interparticle interactions overcome the weaknesses displayed by individual NPs. However, previous studies have considered NP assemblies as inanimate, which had led to their dynamic properties being overlooked. Animate properties, i.e., those mimicking biological properties, endow NP ensembles with unique and unexpected functionalities for practical applications. In this critical review, we highlight recent advances in our understanding of the properties of NP assemblies, particularly their animate properties. Key examples are used to illustrate critical concepts, and special emphasis is placed on animate property-dependent applications. Last, we discuss the barriers to further advances in this field.

INTRODUCTION

Nanoscience and nanotechnology are among the greatest discoveries and advances in the history of human civilization. Research in these sectors has focused on ways to reduce the size of bulk materials to the nanoscale. Nanoparticles (NPs) display novel behaviors due to their small size, large surface area, boundaries, and quantum effects (*1*, *2*); the physicochemical properties of NPs are very different from those of bulk materials. These unique properties have fueled the development of new fabrication techniques and applications, including catalysts (*3*, *4*), sensors (*5*), devices (*6*), imaging modalities (*7*), batteries (*8*), and biomedical platforms (*9*, *10*). The design and construction of assemblies based on NPs controlled in terms of size, shape, and morphology is an emerging topic because conventional NPs cannot completely fulfill the requirements of many applications (*11*).

Transforming NPs into assemblies is an important area of nanoscience research. There are two main reasons for this: First, the application performance of NPs is always based on collective rather than individual NP performance, so interparticle interactions and structure-property relationships must be studied systematically. The second reason is the very high surface energy of NPs, in turn due to the high specific surface area; this provides a tremendous driving force to decrease the Gibbs free energy (*12*). Energy-driven spontaneous organization of NPs must eventually lead to a large and stable assembly. Controllable and precise synthesis of NP assemblies has been realized by tuning interparticle interactions and modifying assembly strategies. Ensembles of NPs have properties that differ from those of bulk and individual NPs (*13*, *14*). The novel optical, electronic, magnetic, optothermal, and mechanical properties of NP assemblies are attributable to the coupling of and cooperation among individual NPs (*15*). NP assemblies have great potential in practical applications, such as sensing (*16*), energy storage (*17*, *18*), ultrastrong materials (*19*), biodegradable plastics (*20*), adsorption (*21*), catalysis (*22*), and therapies (*23*, *24*).

Great effort has been devoted to tuning and enhancing the physicochemical properties of different types of NP assemblies, and some researchers have noted that NP assemblies also have very interesting dynamic properties (*25*–*27*). Wonderfully, the dynamic properties endow NP assemblies, which mimic biological structures, biological activity with exquisite selectivity, specificity, and adaptability to the constantly changing environment (*28*, *29*). Herein, we define NP assemblies with biological properties as animate NP assemblies, i.e., they actively change their initial state to adapt to changes in their environment by deformation/motion, self-replication, perception, self-regulation, and self-repair, accompanied by the input and output of energy. Animate properties are a special aspect of NP assemblies and always appear simultaneous with the static physicochemical properties. Animate NP assemblies can change their speed, intensity, and mode of interaction with the environment in both space and time. By exploiting these animate properties, great progress has been achieved in various applications, such as catalysis, bacterial capture, imaging modalities, nanomedicine, and actuators.

The importance of NP assemblies is becoming more apparent. Although several reviews have summarized state-of-the art developments, none have focused on the animate properties of NP assemblies (*30*–*32*). Herein, we primarily review recent advances in the field of NP assembly, particularly concerning the discovery of previously unknown dynamic properties. Our review begins with a brief introduction to NPs and NP assemblies and then progresses to a discussion of their inanimate properties (Fig. 1). Then, we focus on applications that leverage the animate properties of NP assemblies. To close, a summary and discussion of future prospects are provided. This review is intended to stimulate further research on animate NP assemblies.

NANOPARTICLES

Research on NPs is one of the fastest-developing fields in chemistry. An NP is a particle having at least one dimension smaller than 100 nm; herein, an NP in the context of this paper is a nanoscale component that in many cases is a nanocolloid (*12*). The various types of NPs include zero-dimensional (0D) NPs (*33*), 1D nanowires (*34*), 2D nanosheets (*35*, *36*), and 3D networks (*37*). Because of the unique nanostructure of NPs, their physicochemical properties are substantially different from those of atoms and bulk crystals, as predicted by Feynman in 1959 (*38*). Their fascinating physicochemical properties account for the explosive growth of NP-based nanoscience and nanotechnology.

[1]Beijing National Laboratory for Molecular Sciences, Key Laboratory of Analytical Chemistry for Living Biosystems Institute of Chemistry, Chinese Academy of Sciences, #2 Zhongguancun, North First Street, Beijing 100190, China. [2]University of Chinese Academy of Sciences, Beijing 100049, China.
*These authors contributed equally to this work.
†Corresponding author. Email: wangtie@iccas.ac.cn

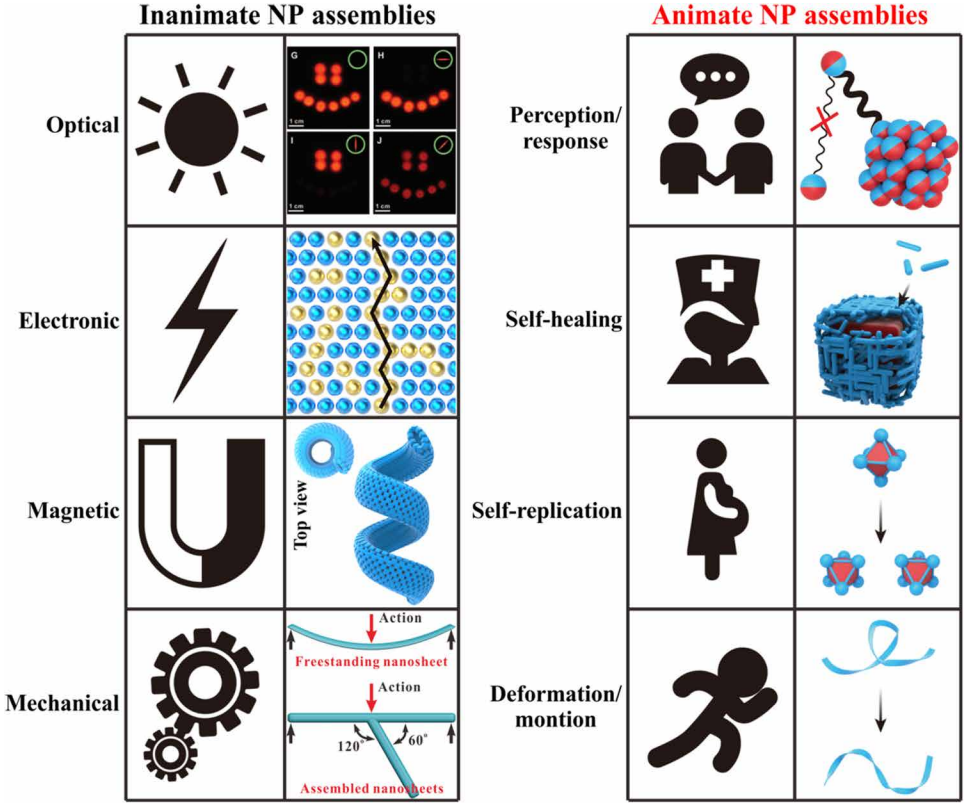

Fig. 1. Schematic diagrams of NP assemblies having inanimate and animate properties. NP assemblies have novel optical, electronic, magnetic, optothermal, and mechanical properties. Reproduced with permission from the American Association for the Advancement of Science (*56*). Emerging animate properties are expected to inspire a new era of NP assemblies.

The size effects that emerge as bulk crystals are transformed into NPs result in important changes in structural, spectroscopic, electronic, thermal, magnetic, mechanical, and chemical properties (Fig. 2) (*39*). Because of their unique physicochemical properties, NPs have achieved great success in a wide variety of applications (*40*). Considering catalysis as an example, the large surface-to-volume ratio and high density of low-coordinated atoms on the surface of NPs render them more active and attractive as catalysts (*41*). Reaction energy can be readily tuned to obtain the highest catalytic activity by controlling the composition, size, and shape of the NPs.

INANIMATE NP ASSEMBLIES

Control of the size and shape of NPs has improved as synthetic techniques have developed. Fundamental research on the assembly of NPs into NP superlattices is of particular interest. If an NP is considered as an "artificial atom," then a superlattice of crystals is, by analogy, an "artificial solid" (*13*). On the basis of the unique and changeable individual driving forces, e.g., entropic forces, and the complex competitive interactions between NPs, various typical superlattices could be formed (*42*). An entire artificial nanoworld has been constructed via this "bottom-up" approach, in which the properties of the individual NPs are preserved along with the properties resulting from the interaction of NPs. Previously unknown properties can also emerge from the strong coupling between assembled NPs. Similar to covalent bonds between atoms in molecules, coupling of surface plasmons, excitons, and magnetic dipoles between adjacent NPs is seen in assemblies (Fig. 3A). For example, inspired by the concept of "symmetry-interaction self-assembly," Lou and co-workers constructed a frame-like superstructure via the assembly of nanocuboids. On the basis of the inherent preferences for particular geometries and dipole-induced electrostatic interaction, this oriented attachment-involved assembly realizes a nanoscale analog to the bonding behavior in supramolecular cubes (*43*). Strong interparticle coupling leads to changes in electronic states, energy levels, confines electromagnetic and magnetic state (Fig. 3, B to F) (*44*–*47*). Another type of interaction between assembled NPs resembles the ionic bond between positive and negative ions (Fig. 4A). Cooperative and complementary structural properties emerge when hard NPs assemble with soft ligands (*12*, *48*). For example, a bone-like hierarchically staggered nanostructure, produced by periodically depositing hydroxyapatite NPs in the gap zones of collagen fibrils during biomineralization, shows an excellent combination of toughness and strength (Fig. 4, B to H) (*49*–*51*). The unique mechanical properties attributed to the hierarchically staggered architecture include resistance to fracture and high energy dissipation. Recently, Yu and co-workers (*52*) fabricated bulk synthetic nacre from brittle aragonite $CaCO_3$ and organic materials (Fig. 4, I to K). Because of its hierarchical structure, the synthetic nacre displayed excellent fracture toughness and ultimate strength.

The properties of assemblies are strongly related to the packing density and ordering of the NPs and to the shape and architecture of the assembled structure. For example, the cross-assembled 2D nanosheet structure effectively distributes stress and strain, thereby

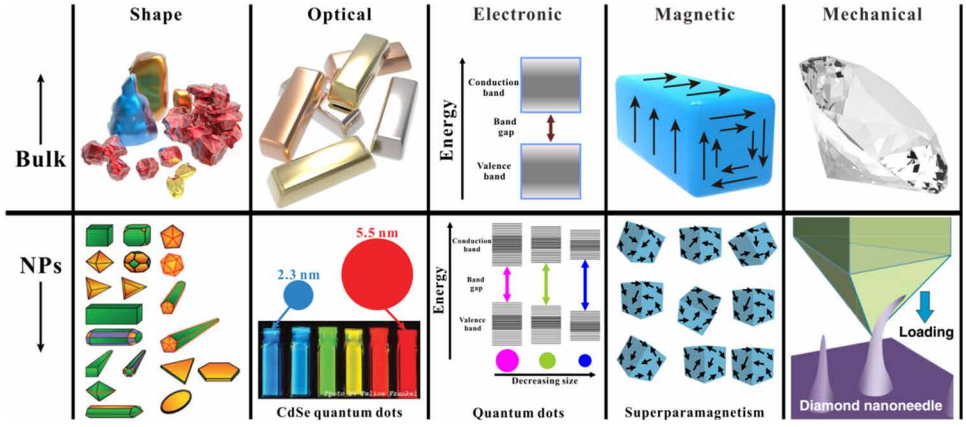

Fig. 2. Comparison between bulk materials and NPs. Compared with bulk materials, NPs can have very different shape, optical, electronic, magnetic, and mechanical properties (left to right). Reproduced with permission from John Wiley and Sons (*108*). Reproduced with permission from the American Chemical Society (*109*). Reproduced with permission from the American Association for the Advancement of Science (*110*).

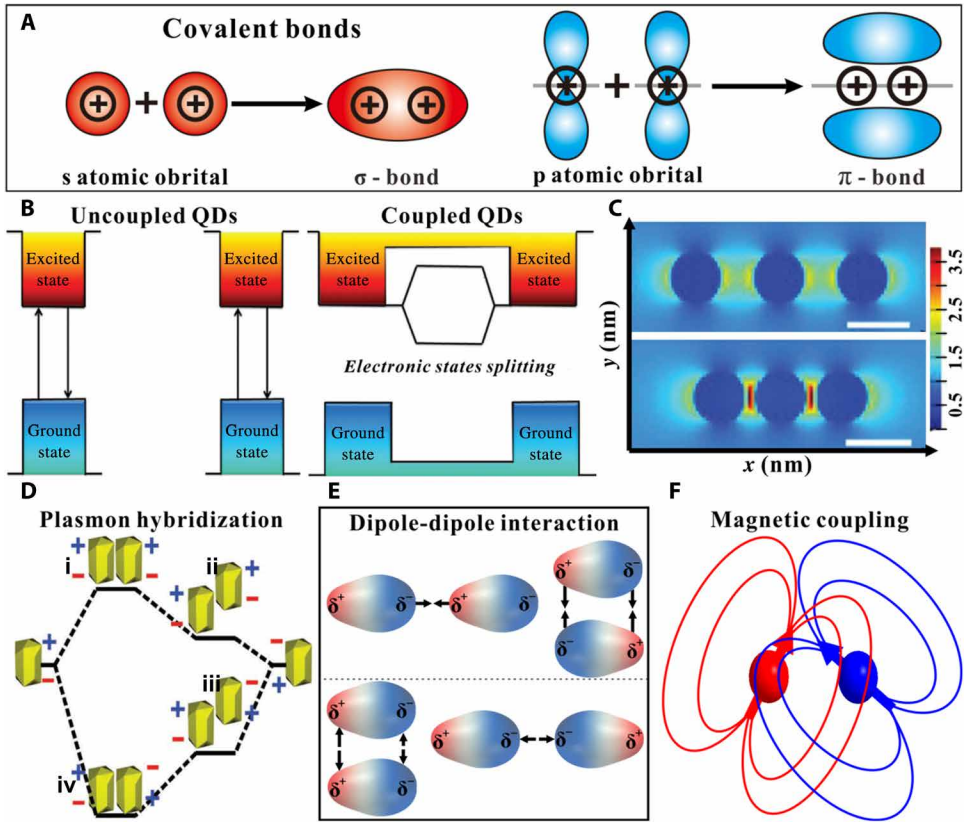

Fig. 3. Covalent bond-type coupling between assembled NPs. (**A**) Covalent bonding between atoms in molecules. (**B**) Energy states of coupled and uncoupled quantum dots (QD). (**C**) Electromagnetic coupling between adjacent NPs in ordered arrays (top) and NP assemblies (bottom). (B) and (C) are reproduced with permission from John Wiley and Sons (*44*). (**D**) Schematic diagrams of plasmon hybridization of the dipoles. Reproduced with permission from John Wiley and Sons (*45*). (**E**) Schematic diagrams of dipole-dipole interactions. (**F**) Schematic diagrams of dipolar interactions between magnetic NPs.

enhancing the mechanical stability of nanosheet assemblies. A wide variety of architectures have been constructed via coupling interactions linking building blocks or by modulating their agreement pattern, leading to completely different functionalities. The enhanced properties of NP assemblies compared with individual NPs can provide previously unidentified solutions for practical applications. To date, novel optical, electronic, magnetic, optothermal, and mechanical properties of NP assemblies have been demonstrated.

Optical properties

Precisely arranging functional nanoscale architectures in 3D provides NP assemblies with optical properties that are difficult or even

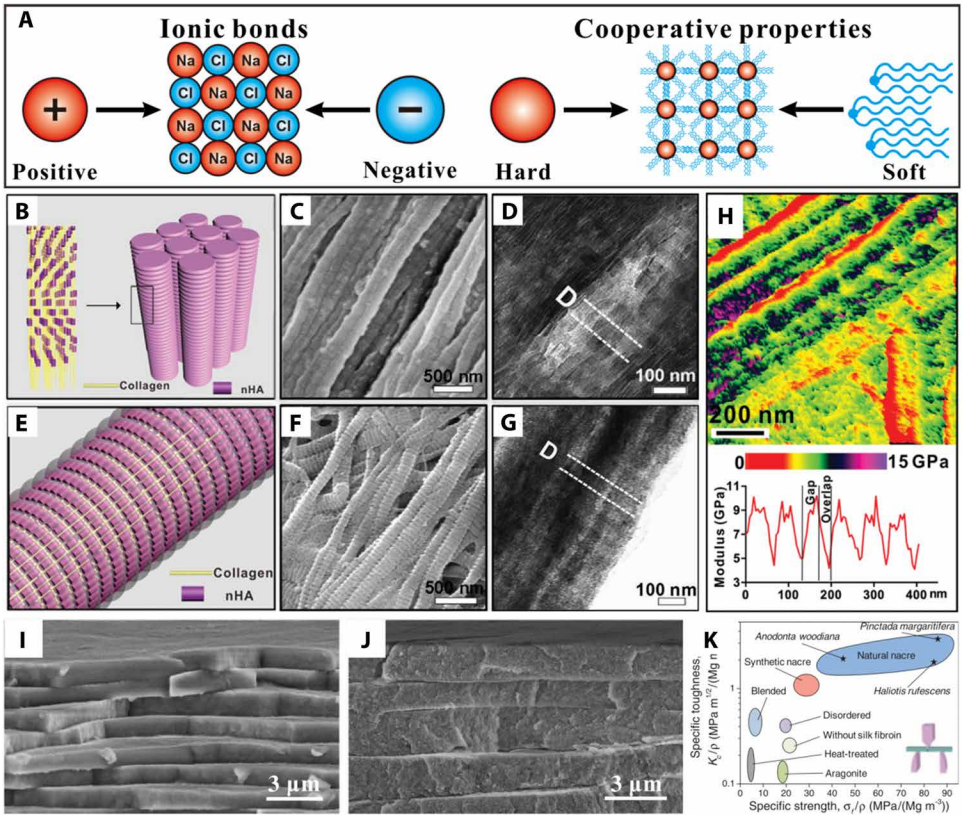

Fig. 4. Ionic bond–type interactions in assemblies. (**A**) Ionic bonding between atoms in crystals and the assembly of hard NPs with soft organic ligands. (**B** to **D**) Schematic diagrams, scanning electron microscopy (SEM) images, and transmission electron microscopy (TEM) images of native bone, respectively. (**E** to **G**) Schematic diagrams, SEM images, and TEM images, respectively, of hierarchical intrafibrillarly mineralized collagen synthesized by a polyacrylic acid–calcium intermediate. (B) to (G) are reproduced with permission from John Wiley and Sons (*49*). (**H**) Atomic force microscopy property maps (top) and sectional Young's modulus analyses (bottom) of hierarchical intrafibrillarly mineralized collagen. Reproduced with permission from John Wiley and Sons (*50*). (**I** and **J**) Surface SEM images of *Anodonta woodiana* nacre and synthetic nacre, respectively. (**K**) Mechanical performance of different materials. (I) to (K) are reproduced with permission from the American Association for the Advancement of Science (*52*).

impossible to achieve in bulk. Conceptually, the optical properties of an ordered plasmonic assembly are based on a collection of interacting dipoles. The individual dipolar particles can interact with each other in an assembly, which can be considered as a "sea of dipoles" with unique material properties. Mirkin and co-workers (*47*) explored how NP assembly influences the optical properties of nanomaterials by developing a "DNA-programmable assembly strategy" to finely control the interior NP architecture. The dipole-dipole coupling between the NPs was changed by tuning the spacing between gold NP building blocks so that the plasmonic superlattices transformed into primarily plasmonic or photonic entities. Their work required in-depth understanding of plasmonic-photonic interactions and provided a useful guide for the design of specific superlattices having preconceived optical properties. The coupling of coherent dipoles also existed in some assemblies made from semiconductor NPs, and the dipole-dipole coupling would notably affect the optical properties of NP assemblies (*53*, *54*).

In addition to novel optical properties, precisely arranging the structure of NP assemblies can also lead to improved optical performance (*55*). For example, Luo *et al.* (*44*) demonstrated that the barrier to electron transfer was overcome when the interparticle spacing was sufficiently small. Interparticle coupling, facilitated by decreased interparticle distance, leads to electronic state splitting and the hybridization of energy levels. The assemblies of Luo *et al.* exhibited distinct optical properties and enhanced electronic energy transfer. Furthermore, the photocatalytic activity of the ordered assemblies was about 10 times higher than that of ordered arrays (Fig. 5, A to E). Wang *et al.* (*56*) found that electric dipole coupling effects among NPs inside superparticles (SPs) can influence photoluminescence anisotropy. CdSe-CdS nanorods, self-assembled into single domains as elongated needle-like SPs (Fig. 5F), exhibited a larger photoluminescence anisotropy ratio than that of individual CdSe-CdS nanorods (Fig. 5, G to I).

Electronic properties

The electronic performance of NP assemblies depends not only on the intrinsic properties of the NPs but also on their surface properties, geometrical arrangement, and connections within the assemblies. Ensembles of NPs can have electronic properties that are quite different from those of discrete NPs, due to the coupling of individual NPs.

Murray and co-workers (*57*) reported that the electronic properties of superlattices are highly tunable and strongly affected by the presence and density of NP dopants. They demonstrated impressive electronic coupling between Au nanocrystal dopants and the CdSe nanocrystals in the superlattice. The presence of the Au NPs markedly increased the conductivity of the semiconductor NP superlattices: The direct-current

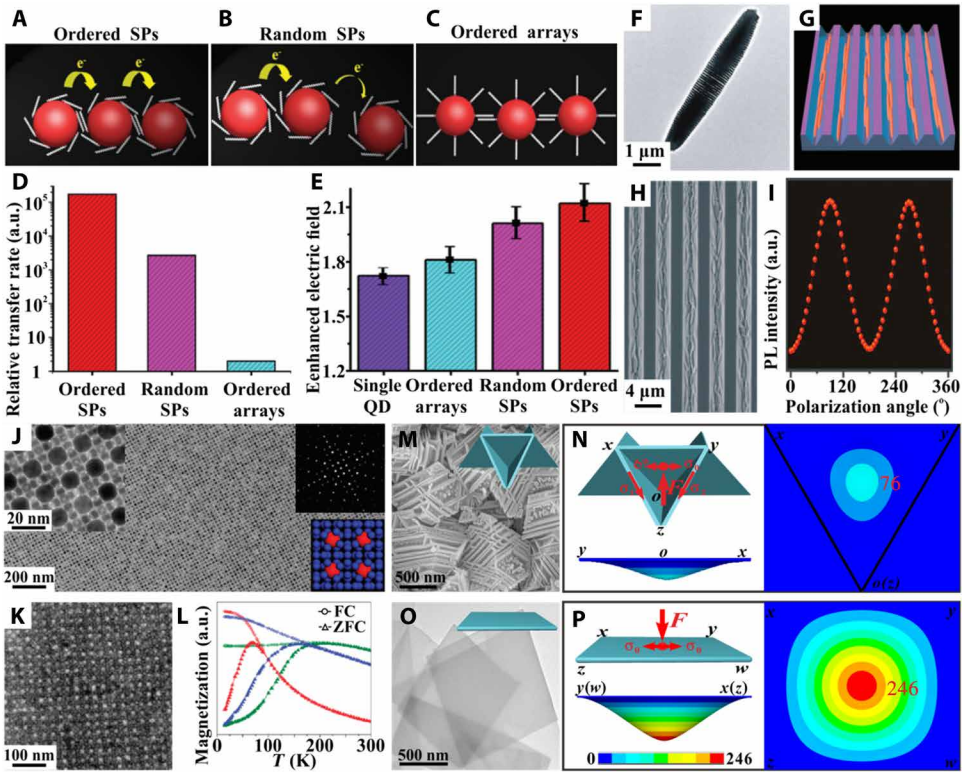

Fig. 5. General physicochemical properties of NP assemblies. (**A** to **C**) Schematic diagrams of intraparticle electronic energy transfer in ordered superparticles (SPs), random SPs, and ordered arrays, respectively. (**D**) Simulated relative intraparticle transfer efficiency. (**E**) Calculated average enhanced electrostatic field intensity. (**F**) TEM image of needle-like CdSe-CdS superlattices. (A) to (E) are reproduced with permission from John Wiley and Sons (*44*). (**G** and **H**) Schematic diagrams and SEM image of unidirectionally aligned needle-like SPs, respectively. (**I**) Dependence of photoluminescence intensity on polarization angle. (F) to (I) are reproduced with permission from the American Association for the Advancement of Science (*56*). (**J**) TEM image of binary Fe_3O_4 nanocrystal superlattices. Insets: Magnified image, corresponding selected area electron diffraction patterns, and structural model. (**K**) SEM image of binary Fe_3O_4 nanochain superlattices. (**L**) Zero field–cooled and field-cooled magnetization curves for the 7.2-nm Fe_3O_4 nanocrystals (red), 14.3-nm Fe_3O_4 nanocrystals (olive), and binary Fe_3O_4 nanocrystal superlattices (blue). (J) to (L) are reproduced with permission from the American Chemical Society (*46*). (**M**) SEM image of the nanosheet assemblies. (**N**) Nanosheet assembly model and its calculated displacement distribution profile. (**O**) TEM image of the nanosheets. (**P**) Nanosheet model and its calculated displacement distribution profile. (M) to (P) are reproduced with permission from the Nature Publishing Group (*3*). a.u., arbitrary units.

conductivity of 16.5% Au/Ag-doped PbSe superlattices was six orders of magnitude higher than that of pure PbSe NPs.

In another example, Cao *et al.* (*58*) assembled semiconducting single-walled carbon nanotubes (SWCNTs) into aligned arrays with full surface coverage via the Langmuir-Schaefer–based method. The intrinsic mobility of the nanotubes was preserved after array assembly. Thus, coupling of the 99% pure semiconducting CNTs and the high packing density resulting from high alignment accuracy provided arrays with notably improved electrical properties and device performance.

Magnetic properties

In applications, magnetic assemblies of NPs are more controllable than individual NPs because of their more sensitive magnetic response, enhanced magnetic properties, and increased number of multivalent interactions (*59*). After the evidence of magnetic dipoles was found in the arrays of magnetic NPs made by the Langmuir method, Murray and co-workers studied systematically interparticle dipolar interactions in binary NP superlattices (*46*, *60*). Dipole-dipole interactions between two differently sized Fe_3O_4 NPs in binary NP superlattices induced an additional energy barrier, where the magnetic moments of the smaller Fe_3O_4 were pinned by the local dipolar field induced by the random magnetic moments of the larger Fe_3O_4 NPs (Fig. 5J). The binary NP superlattice membranes displayed single phase–like magnetization alignment, which was not observed in the phase-separated NP mixtures (Fig. 5, K and L). Wen and co-workers provided another example involving dipole-dipole interactions between magnetic NPs in NP assemblies (*61*). They found that the magnetic properties of Ni-Co alloy NP assemblies could be differentially "tuned" by altering the material composition. Controllable self-assembly was enabled by the strong magnetic moment of the NPs and external magnetic field. Moreover, saturation magnetization of NP assemblies exhibited a "roller coaster" effect when the molar ratio of Ni/Co in the Ni-Co alloy NPs was changed.

Optothermal properties

The NP assemblies play a vital role in the development of energy technology, and photothermal conversion is one of the most representative applications (*62*). Controlled assembly is the method of choice for scalable nanomanipulation of the optothermal properties of NPs. Interparticle plasmonic coupling can provide NP assemblies with notably improved photothermal efficiency (*63*). Gold NPs display strong photothermal effects that have been widely investigated in the context of plasmonic photothermal therapy. To address the

problems associated with single gold NPs, Chen and co-workers (*24*) provided a novel solution whereby self-assembly of gold NPs into biodegradable gold vesicles shifted the surface plasmon resonance to the near-infrared region. The self-assembly process enabled dense packing of the gold NPs, which led to ultrastrong plasmonic coupling between adjacent gold NPs. This resulted in an obvious redshift in the extinction spectrum. The photothermal conversion efficiency of the biodegradable gold vesicles was 37%, which is markedly higher than that of gold nanorods (22%) and gold nanoshells (13%). A similar effect was reported by Gao and co-workers (*23*), who found that assembly caused the surface plasmon resonance peak to shift to a longer wavelength. In their research, the absorption maximum of gold NP assemblies extended to the near-infrared region of 700 to 900 nm, while the absorption peak of the isolated NPs appeared near 520 nm. The gold NP assemblies displayed remarkable photothermal ablation and had negligible cytotoxicity.

We recently reported that assembling high-quality Cu_7S_4 NPs into a dense film greatly enhanced the water evaporation rate in light-induced water evaporation (*64*). The maximum photothermal conversion efficiency was 77.1%, which was much higher than that of the monodispersed NPs. The performance improvement was attributed to the ability of the NP assemblies to change the mechanism of vapor transport.

Mechanical properties

The mechanical strength and modulus of nanomaterials depend strongly on the inherent mechanical properties and are affected by the interior structure, especially the interfacial contact distribution and the associated interfacial interactions (*48*). Designing and constructing assemblies with a desirable microstructure could greatly enhance mechanical performance, while also retaining the excellent properties of the pristine NPs. We recently reported that 3D-stacked metal-organic framework (MOF) nanosheets had much better structural stability than freestanding MOF nanosheets (*3*). Taking inspiration from the honeycomb, whose good mechanical properties result from a hexagonal structure, a stacked-nanosheet superstructure formed via an exquisite etching strategy had nanosheets intersecting at a perfect 60° angle (Fig. 5M). When one side of the triangle was stressed, the other two sides provided counteracting stresses to minimize structural deformation. Simulation results revealed that the displacement of a freestanding MOF nanosheet was over three times greater than that of stacked MOF nanosheets under the same external stress (Fig. 5, N to P). Experiments confirmed that the stacked MOF nanosheet framework was maintained after five successive catalytic cycles, while notable breakage and agglomeration of fragments occurred with the monodispersed nanosheets. Lu and co-workers (*65*) reported 3D honeycomb-like assemblies having exceptionally high mechanical stability. The well-organized assemblies containing three types of polygonal nanopores, i.e., trihedral, quadrangular, and pentagonal, were prepared via a novel interfacially reactive self-assembly process. The mechanical stability of the trihedral nanopore structure, and the deformability of the other polygonal nanopores, provided the graphene assembly with an elastic modulus that far exceeded those of other graphene-based assemblies.

The outstanding mechanical properties of certain biological materials are attributed to their hierarchically ordered structures at multiple levels. Biomimetic assembly of high-quality nanoplatelets into hierarchically ordered structures could be an efficient route to realizing high-performance macroscopic films. For example, Yu and co-workers (*52*) fabricated bulk synthetic nacre via a novel mesoscale "assembly and mineralization" approach. The composition and interior structure of the synthetic nacre and natural nacre were very similar. The synthetic nacre displayed much better mechanical performance than pure aragonite $CaCO_3$ nanoplatelets and related composites. Rational assembly of hard NPs into assemblies upon addition of soft ligands is also an effective way to enhance the mechanical properties of materials (*66*). Wang *et al.* (*67*) found that the structural stability, elastic strength, and fracture toughness of 2D CdSe nanosheets with surface-ligand bonding are much better than that without surface-ligand bonding. The dramatic elevation of mechanical stability should be attributed to the presence of surface-bonded soft organic ligands undoubtedly.

Superwettable properties

Superwettability is a unique phenomenon that is determined by the chemical component on the surface and multiscale micro-nano structure of material (*68*). Assembled NPs to cover the material's surface with desired pattern of structure can effectively control its wettability. Recently, Jiang and co-workers (*69*) demonstrated that the nanostructured MoS_2 film assembled by MoS_2 nanoplatelets presents strong underwater "superaerophobic" property. The constructed superaerophobic electrode surface shows an extremely low contact area with the gas bubbles, leading to an extremely low adhesive force to the surface. Thanks to the in-time leaving of as-formed H_2 bubbles, the nanostructured MoS_2 film demonstrates much higher hydrogen evolution performance than the flat MoS_2 film. Wang and co-workers (*70*) also found that while the synthesized platinum NPs were assembled into striped-pattern superlattices on the electrode, they would cause the electrode to exhibit superaerophobicity. The under-electrolyte superaerophobicity facilitates the disengagement of as-formed gas bubbles from electrode surface with ease, contributing to a notable boost in hydrogen evolution reaction effectiveness.

ANIMATE NP ASSEMBLIES

The dynamic properties of NP assemblies have been subject to considerably less study than their general physicochemical properties. Previous studies indicated a close relationship between the animate and dynamic properties of NP assemblies. Similar to organisms that can actively respond to external stimuli, intelligent NP assemblies can also engage in deformation/motion, self-healing, perception/response, and self-replication processes.

Motion properties

Motion is a fundamental aspect of life. Mobile NP assemblies exhibit enhanced flexibility and functionality compared with static NP assemblies. The various types of mobile NP assemblies include electrically powered, magnetism-driven, external force–driven, photo-induced, and shape memory–induced assemblies.

Electrically powered motion

Propelling NP assemblies in a controlled manner is challenging because it requires conversion of electrical energy into motion. Electronic excitation of mobile NP assemblies can result in excitation-induced geometrical changes and sequential configurational and conformational switching. For example, actuation of a CNT aerogel from the static to dynamic condition has been reported using external electrical stimuli. Baughman and co-workers (*71*) fabricated CNT

aerogel sheets from forests of multiwalled CNTs. The aerogels had gas-like density with low modulus and high elongation. Application of an electrical stimulus to the high–aspect ratio single sheet led to charge-induced actuation, expressed as expansion in the width and thickness directions but contraction in the length direction.

Magnetism-driven motion

Magnetism remains the most convenient way to enable magnetic NPs to move under the application of an external magnetic field during chemical and biological reactions. Magnetism-driven motion of NP assemblies has led to achievements that are impossible for conventionally sized devices, e.g., magnetic spin bars for mixers in nanoscale reactors (Fig. 6A). Chen and co-workers (*72*) constructed a nanometer-sized magnetic stirring bar by assembling Fe_3O_4 NPs into a single-line nanochain (Fig. 6, B and C). The rigid Fe_3O_4 nanochains immediately responded to a common magnetic stirring plate and could be rotated rapidly within small droplets (Fig. 6D).

External force–driven motion

Soft macroscopic materials are readily transformed by external forces. A similar phenomenon also occurs in the microworld. Softening NPs is the most straightforward way to realize this ability because the NPs can then dynamically deform in the environment. Both top-down and bottom-up methods are used to prepare the assemblies. The top-down strategy involves superfining or ultrathinning bulk NPs into 2D/1D NPs that have low Young's modulus and hardness. Then, the flexible NPs are assembled into forms that have a suitable shape and size to maintain the desired deformation. The bottom-up strategy assembles monodispersed NPs into high–aspect ratio 2D NP assemblies. These 2D NP assemblies, i.e., nanochains, are also deformable.

Photoinduced motion

Phototaxis, which is commonly observed among motile microorganisms in nature, can also be used to stimulate and guide the motion of NP assemblies. When illuminated, photoactive assemblies consume surrounding fuel and exhibit autonomous motion in the desired direction. Tang and co-workers (*73*) provided an excellent example involving the fabrication of a light-driven microswimmer based on a Janus TiO_2/Si nanotree. In their structure, a single-crystal Si nanowire served as the photocathode and a single-crystal TiO_2 nanowire was used as the photoanode. Exposure to light generated an asymmetric distribution of charged reaction products along the nanotree axis, which propelled the microswimmer via electrophoresis. Positive or negative phototaxis could be induced by changing the zeta potential of the Janus nanotree via suitable chemical treatment, to alter the migration speed and direction.

Shape memory–induced motion

The shape memory property endows certain NP assemblies with the ability to return to their original shape after deformation, when the external conditions change. Typically, the assemblies are firstly programmed into a temporary shape, and then they recover into the original shape. Wu and co-workers (*74*) reported the synthesis of sponge-like CNT assemblies having a lightweight, high-porosity, and large surface area. The CNT sponges could be elastically deformed into many shapes without breaking. Moreover, the sponges largely recovered their original shapes, both in air and liquids, even under large-strain deformations. Islam and co-workers (*75*) reported the assembly of SWCNTs into an aerogel, which was then coated with graphene nanoplatelets. The assemblies displayed excellent structural robustness after 1×10^6 compression and release cycles, and the original shape was recovered very quickly after removal of the load.

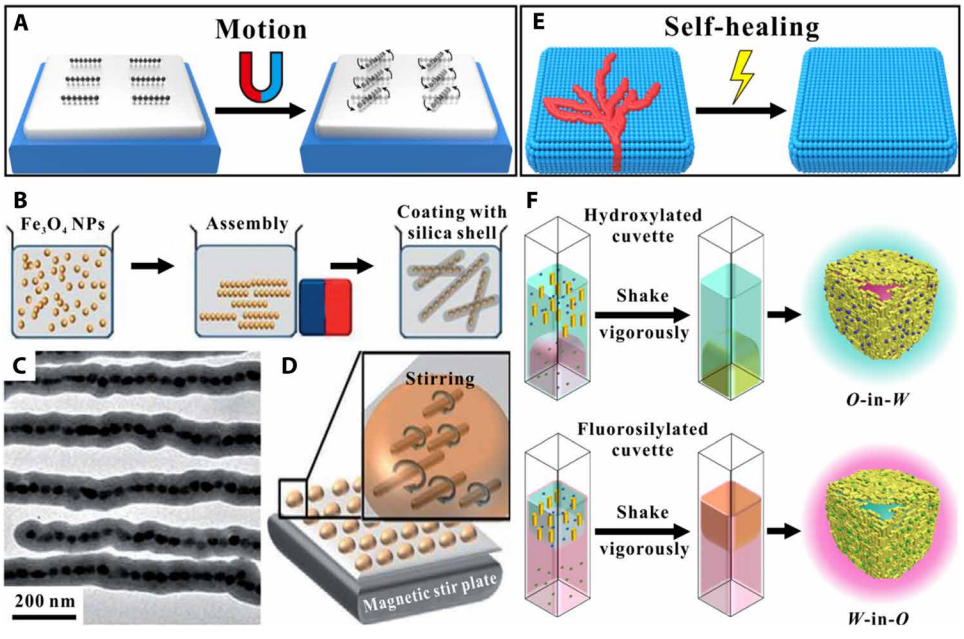

Fig. 6. Animate properties of NP assemblies. (**A**) Schematic diagrams of NP assembly motion under an applied external magnetic field. (**B**) Synthesis and (**C**) TEM image of nano-sized stirring bars. (**D**) Schematic representation of the parallel stirring of droplets on a magnetic stir plate. (B) to (D) are reproduced with permission from John Wiley and Sons (*72*). (**E**) Schematic diagrams of self-healing properties. (**F**) Schematic diagram of the self-assembly of metal liquid–like 3D gold nanorod arrays. Reproduced with permission from the Nature Publishing Group (*77*).

Self-healing properties

Self-healing is an important ability for living organisms. In NP assemblies, this ability endows them with enhanced robustness in practical applications (Fig. 6E) (*76*). Tan and co-workers (*77*) developed a reversible chloroform/water casing material to realize self-healing metal liquid–like 3D gold nanorod arrays (Fig. 6F). The arrays were always located at the chloroform/water interfaces, which ensure that they were self-healing and defect free. Introduction of reversible bonds or interactions in NP assemblies are another way to endow them with the self-healing ability. Yu and co-workers (*78*) created dynamic Ag—S bonds in an Ag nanowire aerogel framework that had self-healing capability. Rapid and strong deformation/reformation of the dynamic Ag—S bonds under near-infrared laser irradiation provided a healing efficiency of 93%.

Perception/response properties

Individuals can be organized into a group through a delicate balance of attractive and repulsive interactions. The dynamic responses among individuals lead to complex collective behavior, whereby the group displays an abundance of diverse spatiotemporal patterns. The individuals would change their space, orientation, and velocity depending on their own perceptions, and different states can be dynamically switched in the group. Similarly, Palacci *et al.* (*79*) designed and constructed 2D "living crystals" based on a dynamic assembly process underpinned by competition between attractive interaction of particles and self-propulsion. The living NP assemblies could form, break, explode, and reform depending on light-induced nonequilibrium collisions of the self-propelled particles. Lavergne *et al.* (*80*) found that the dynamic collective behavior of active particles had a strong relationship with the visual perception/response of individuals. Jiang *et al.* (*81*) demonstrated that 1D superparamagnetic magnetite arrays with magnetic field perception can be fabricated to mimic the magnetosensing behavior seen in nature. To construct assemblies that have high magnetization anisotropy, a bottom-up liquid processing method was used to obtain high–aspect ratio 1D Fe_3O_4 NP arrays. Magnetization curves confirmed the high magnetization anisotropy of the arrays and the ability to perceive magnetic fields.

Self-replication properties

Self-replication is a hallmark of life. Understanding and realizing self-replication in nanomaterials would constitute a paradigm shift in materials discovery that could revolutionize material science and nanotechnology. Self-replication is an important characteristic of dissipative self-assembly (Fig. 7A). When the surrounding environment is far from thermodynamic equilibrium, the temporal dynamics and spatial arrangements of NPs in assemblies are always changing, which facilitates self-replication. Yan and co-workers (*82*) presented a dissipative colloidal solution system whose optical binding strength and system entropy were critical for the self-replication of dimer units (Fig. 7B). In linearly polarized light, the dissipative silver NP colloidal system transitioned spontaneously from a disordered to an ordered state. The transition led to self-replication, i.e., the formation of one dimer triggered the formation of more dimers, which, in turn, led to the collapse of hexagonal lattice structures. Such light-induced

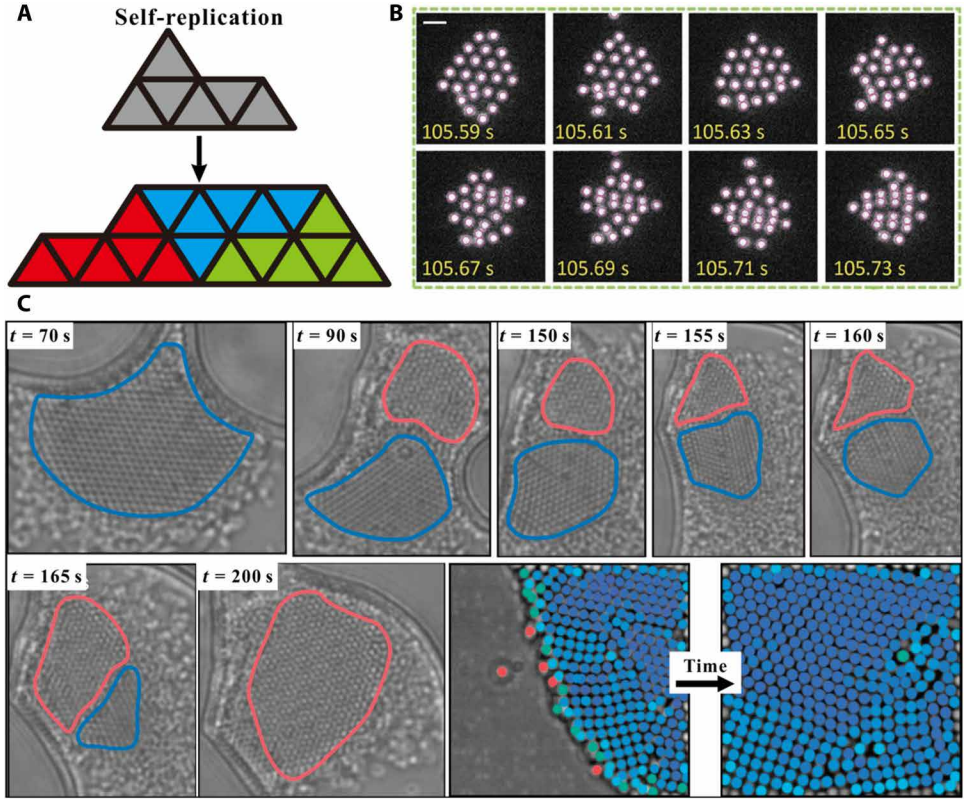

Fig. 7. Self-replication properties of NP assemblies. (**A**) Schematic diagrams of self-replication properties. (**B**) Dark-field images showing the formation of several Ag dimer chains. Reproduced with permission from John Wiley and Sons (*82*). (**C**) Time-lapse images of the self-replication process of assemblies. Reproduced with permission from the Nature Publishing Group (*83*).

self-organization is a promising strategy to reconfigure nanoscale building blocks into novel architectures. Dissipative self-assembly can be used for experimental study of the replication process of a given structure. In general, a process is regarded as self-replicating in a system that is not in thermodynamic equilibrium, but is described as crystal growth in a system in thermodynamic equilibrium. Ilday *et al.* (*83*) used ultrafast laser pulses to create spatiotemporal temperature gradients, which induced Marangoni flow to drive the assembly of NPs. Impressively, the hexagonal lattice gradually transformed into a Moiré pattern, which then self-replicated and self-reproduced to fill the available area (Fig. 7C). The NP assemblies could be separated into two groups that have the same pattern; alternatively, one large assembly could be detached and used to form the same pattern in another location.

APPLICATIONS OF ANIMATE NP ASSEMBLIES

As noted above, animate NP assemblies have the general physicochemical properties of assemblies and are also endowed with unique animate properties. It is these animate properties that make them of particular interest for applications including catalysis, imaging, bacterial capture, nanomedicine, and actuators. In this section, the applications of various animate NP assemblies are discussed with an emphasis on (i) the creation of animate properties in NP assemblies by rational design of their compositions, morphologies, and hierarchical structures, and (ii) the advantages of animate NP assemblies compared with inanimate NP assemblies.

Catalysis

Heterogeneous catalytic reactions involve three steps: adsorption of reactants, reaction of adsorbed species, and desorption of products (*84*). Mass transfer and catalytic activity must both be adjusted for optimal catalytic performance. Xu and co-workers (*85*) synthesized a series of bioinspired inner-mobile arrays whose artificial cilia mimicked natural ciliary motion; beating of the cilia was assisted by internal magnetism and external magnetic fields. The arrays exhibited the unique ability of microfluidic manipulation. The vortex generated by each cilium enhanced the mixing performance and accelerated mass transfer in the entire system. The photocatalytic performance of the mobile arrays was about three times better than that of static arrays.

Animate NP assemblies stimulate mass transfer to overcome diffusion limitations and create dynamically confined spaces that enhance chemical reactivity. Klajn and co-workers (*86*) found that dynamic self-assembly could notably accelerate reactions and influence stereoselectivity. During the assembly process, reactant molecules from the surrounding bulk solution are trapped inside cavities (Fig. 8A). The entrapment effectively increases molarity and/or functions as a form of preorganization by trapping reactant molecules and thus accelerating their reactivity. At reaction completion, the NP assemblies were disintegrated by irradiation with visible light. This released the products and established a new catalytic cycle. The stereoselectivity of the reaction could be altered by adjusting the chemical reactivity of the species trapped within the dynamic assemblies.

Imaging

Magnetic resonance imaging, which is a noninvasive clinical diagnostic technique, uses gadolinium oxide NPs as contrast agents to improve imaging sensitivity (*87*). However, traditional imaging nanoprobes suffer from low biocompatibility and high toxicity, induced by nonspecific adhesion of proteins and endocytosis (*88*). The application of animate NP assemblies with modifiable configurations could mitigate these issues. For example, Luo *et al.* (*7*) fabricated anisotropic assemblies of ultrathin gadolinium oxide nanocoils that exhibited low Young's modulus and stiffness and were much softer than other nanomaterials such as NPs, nanotripods, and nanodisks. In solution, the nanocoils showed a change in their spatial configuration such that the increased steric hindrance suppressed nonspecific protein adhesion (Fig. 8B). Moreover, the transformable nanocoils exhibited steric repulsion and cellular internalization, which improved their biocompatibility. In vivo magnetic resonance imaging experiments confirmed that the ultrathin gadolinium oxide nanocoils effectively prolonged the image enhancement time.

Bacterial capture

Animate 3D NP assemblies having the characteristic of deformability show promise as bioinspired nanoclaws for the capture of bacteria. During extracorporeal blood cleansing therapy, the high shearing force generated by the high flow velocity of the bloodstream leads to low bacterial capture efficiency due to weak interaction forces between the bacteria and the 3D nanostructures. Simulating the predatory strategy of the Venus flytrap, Liu *et al.* (*89*) designed 3D nanoclaws based on an array of nanowires (Fig. 8C). The relatively low Young's modulus of the nanowires enabled them to elastically deform into a bent shape. The initially soft and straight nanowires instantly bent to close the trap whenever the target bacteria touched the nanowire arrays (Fig. 8D). Nanowire deformation was induced by the strong adhesive force of bacteria, which was sufficient to prevent trapped bacteria from escaping. The bacterial capture efficiency of the 3D nanoclaws was more than twice that of unbendable nanowire arrays (Fig. 8E).

Nanomedicine

NPs have great potential in nanomedical applications. For example, they can prolong circulation half-life and enhance permeability during drug delivery (*90*, *91*). The design and construction of suitable nanocarriers are important for improving treatment efficacy and reducing side effects. The dynamic deformability and strong perception/response ability of animate NP assemblies are highly advantageous for nanomedical applications. Zhao *et al.* (*92*) reported a novel near-infrared light–responsive decomposable nanocapsule, fabricated via layer-by-layer self-assembly and up-/down-conversion of NPs and light-responsive polymers, for drug delivery. The large assemblies enabled the blood circulation time to be extended and greatly enhanced tumor accumulation. Moreover, illumination with near-infrared light decomposed the nanocapsule, which allowed rapid elimination from the tumors and release of the loaded chemotherapy drugs. Lu and co-workers (*9*) also found that deformable NP assemblies were beneficial for drug delivery. Their intrinsically flexible nanocapsules underwent spherical-to-oval deformation during cellular uptake, which was enhanced 26-fold compared with nondeformable nanocapsules. Moreover, deformable nanocapsules loaded with an anticancer drug exhibited greater ability to kill cancer cells.

Actuators

Actuators convert external energy into mechanical displacement; they are widely used in electromechanical systems, robotics, and artificial muscles, and for sensing. An animate NP assembly having a flexible

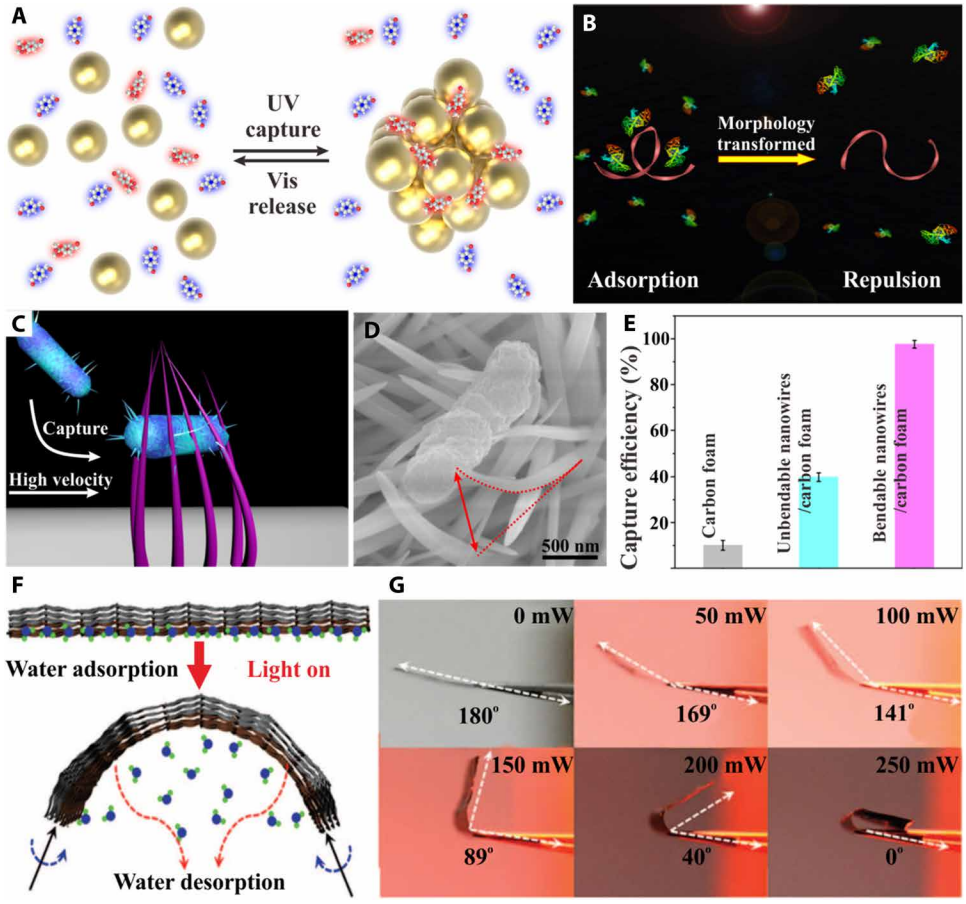

Fig. 8. Applications of animate NP assemblies. (**A**) Schematic diagram of the reversible trapping of molecules. (**B**) Schematic diagram of the interaction between proteins and a nanocoil. Reproduced with permission from the American Chemical Society (*7*). (**C**) Bacterial capture by 3D nanoclaws at high flow velocity. (**D**) SEM image of polycrystalline nanowires during bacterial capture. (**E**) Bacterial capturing efficiencies of different dialyzers. (C) to (E) are reproduced with permission from the Nature Publishing Group (*89*). (**F**) Schematic diagram of the actuation mechanisms of graphene paper. (**G**) Bending angle as a function of irradiation intensity. (F) and (G) are reproduced with permission from the American Association for the Advancement of Science (*93*). UV, ultraviolet; Vis, visible.

structure, strong self-repairing ability, and sensitivity toward external stimuli is a good actuator candidate. Several types of soft NP assemblies have been shown to have excellent actuation performance; these include origami-inspired graphene-based paper (Fig. 8F) (*93*), graphene oxide paper (*94*), 2D metallic molybdenum disulfide film (*95*), NiOOH fibers (*96*), V_2O_5 fibers (*97*), and vanadium dioxide/SWCNT films (*98*). Graphene oxide was used as nanoscale building blocks to fabricate the graphene-based paper, which showed fast response times and excellent light sensitivity. The graphene paper was programmed to have a dual gradient (vertical and lateral) structure and exhibited self-folding behavior upon irradiation with near-infrared light. Remotely controlled by gentle illumination or heating, the graphene paper–based device can produce predesigned shapes, walk, and turn a corner (Fig. 8G). The 2D metallic molybdenum disulfide nanosheets assembled into a soft electrode film performed well in terms of shape morphing (*95*). The electrode film exhibited dynamic expansion and contraction, attributable to electrochemically mediated insertion and removal of cations between the nanosheets. The expansion was exploited for actuation, allowing the electrode to lift more than 150 times its own weight. The mechanical stresses generated by the molybdenum disulfide film were much higher than those generated by mammalian muscle, being comparable to those of ceramic piezoelectric actuators.

Biosensor

Assembly of animate NPs also has many applications in bioanalysis and biosensing (*99*–*101*). The rational use of DNA and RNA hybridization can effective construct animate NP assemblies for detection system. Kuang and co-workers (*102*) fabricated DNA-driven graphene oxide–gold NP assemblies with dynamic chiroptical and surface enhanced Raman scattering activities against target molecules. In the detection of microRNA-21 and epithelial cell adhesion molecule (EpCAM), the hybridization of graphene oxide-Au NP structures and microRNA-21 induce release of the label-modified Au NPs from graphene oxide and generate detectable Raman signals, while EpCAM recognition generates circular dichroism signals. Assembly of animate plasmonic NPs to protein is also a good way to construct the detection system. Liz-Marzán and co-workers (*103*) developed a methodology to detect amyloid fibrils down to nanomolar concentrations. The principle is that helical protein fibrils can induce charity assembly of nanorods, which leads to drastic change of circular dichroism signals.

CONCLUSIONS

NP assemblies are evolving from inanimate to animate types. Early research established that NP assemblies possessed numerous novel

properties, of which the most notable was unprecedented strength. Just as the natural world has evolved from inanimate matter to living organisms, so too will NP assemblies doubtlessly evolve into lifelike states. Such a transformation is of interest because it represents a qualitative rather than quantitative change. Animate processes include deformation/motion, self-replication, perception, self-regulation, and self-repair. These processes are always accompanied by an energy change. Animate properties represent a special aspect of NP assemblies. Animate and inanimate properties can coexist within the same assembly. Extensive research has provided a deep understanding of animate NP assemblies, which have physicochemical properties that allow them to mimic living creatures in terms of actively responding to the environment. The unique dynamic properties of higher-dimensional animate NP assemblies provide a broad range of potential applications.

Animate NP assemblies actively respond to the surrounding environment and can change their speed, intensity, and mode of interaction with it in both space and time. According to the modified empirical Shilov equation (*104*, *105*), the adsorption of multicomponent in a dynamic system follows the rule: $\tau = \frac{s \cdot f}{v \cdot c} \cdot h$, where τ is the adsorption capacity, s is the effective contact area, f is the acting force, v is the flow velocity, c is the concentration, and h is the adsorbent layer thickness. If the assemblies can deform and move easily while interacting with the environment, then not only the effective contact area and the interaction forces would be increased but also the flow velocity could be changed, thus promoting the total adsorption capacity of target molecules (*7*, *89*). The development of soft assemblies represents a recent breakthrough in the construction of animate NP assemblies. However, few animate NP assemblies have been reported. In some cases, the presence of animate properties goes unrecognized and thus, unfortunately, unreported. Another apparent barrier to further exploration and discovery of animate properties is the lack of in situ monitoring techniques, such as in situ transmission electron microscopy (TEM) (*106*), Raman imaging, and synchrotron-based x-ray technique (*107*).

The exploration of novel animate properties of NP assemblies, and identifying suitable applications, is as important as their synthesis. A deeper understanding of the structure-property relationships that characterize living organisms may inspire the discovery of novel animate properties. It is of particular interest to expand the applications of NP assemblies to the life and energy sciences. Animate properties can greatly change the speed, strength, and type of interactions between assemblies and the environment, which could lead to previously unknown findings. Precisely tuning the composition, size, and shape of NP assemblies can drastically improve performance while maintaining stability. Last, large-scale production methods for NP assemblies are essential for industrial applications that require large numbers of assemblies. New automated synthetic approaches to realize high reproducibility and mass production will pave the way for intelligent and practical assembly applications. The development of animate NP assemblies is still in its infancy, and many possibilities await exploration.

REFERENCES AND NOTES

1. K. D. Gilroy, A. Ruditskiy, H.-C. Peng, D. Qin, Y. Xia, Bimetallic nanocrystals: Syntheses, properties, and applications. *Chem. Rev.* **116**, 10414–10472 (2016).
2. S. Yip, Nanocrystals: The strongest size. *Nature* **391**, 532–533 (1998).
3. C. Huang, J. Dong, W. Sun, Z. Xue, J. Ma, L. Zheng, C. Liu, X. Li, K. Zhou, X. Qiao, Q. Song, W. Ma, L. Zhang, Z. Lin, T. Wang, Coordination mode engineering in stacked-nanosheet metal–organic frameworks to enhance catalytic reactivity and structural robustness. *Nat. Commun.* **10**, 2779 (2019).
4. P. Zhang, X. F. Lu, J. Nai, S.-Q. Zang, X. W. D. Lou, Construction of hierarchical Co–Fe oxyphosphide microtubes for electrocatalytic overall water splitting. *Adv. Sci.* **6**, 1900576 (2019).
5. S. Zhang, R. Geryak, J. Geldmeier, S. Kim, V. V. Tsukruk, Synthesis, assembly, and applications of hybrid nanostructures for biosensing. *Chem. Rev.* **117**, 12942–13038 (2017).
6. M. S. Saleh, C. Hu, R. Panat, Three-dimensional microarchitected materials and devices using nanoparticle assembly by pointwise spatial printing. *Sci. Adv.* **3**, e1601986 (2017).
7. D. Luo, S. Cui, Y. Liu, C. Shi, Q. Song, X. Qin, T. Zhang, Z. Xue, T. Wang, Biocompatibility of magnetic resonance imaging nanoprobes improved by transformable gadolinium oxide nanocoils. *J. Am. Chem. Soc.* **140**, 14211–14216 (2018).
8. J. Zhang, Z. Li, Y. Chen, S. Gao, X. W. D. Lou, Nickel–iron layered double hydroxide hollow polyhedrons as a superior sulfur host for lithium–sulfur batteries. *Angew. Chem. Int. Ed. Engl.* **57**, 10944–10948 (2018).
9. Z. Teng, C. Wang, Y. Tang, W. Li, L. Bao, X. Zhang, X. Su, F. Zhang, J. Zhang, S. Wang, D. Zhao, G. Lu, Deformable hollow periodic mesoporous organosilica nanocapsules for significantly improved cellular uptake. *J. Am. Chem. Soc.* **140**, 1385–1393 (2018).
10. Z. Wang, H. Liu, S. H. Yang, T. Wang, C. Liu, Y. C. Cao, Nanoparticle-based artificial RNA silencing machinery for antiviral therapy. *Proc. Natl. Acad. Sci. U.S.A.* **109**, 12387–12392 (2012).
11. M. A. Boles, M. Engel, D. V. Talapin, Self-assembly of colloidal nanocrystals: From intricate structures to functional materials. *Chem. Rev.* **116**, 11220–11289 (2016).
12. Z. Xue, C. Yan, T. Wang, From atoms to lives: The evolution of nanoparticle assemblies. *Adv. Funct. Mater.* **29**, 1807658 (2019).
13. N. A. Kotov, F. C. Meldrum, C. Wu, J. H. Fendler, Monoparticulate layer and Langmuir-Blodgett-type multiparticulate layers of size-quantized cadmium sulfide clusters: A colloid-chemical approach to superlattice construction. *J. Phys. Chem.* **98**, 2735–2738 (1994).
14. A. Taleb, C. Petit, M. Pileni, Synthesis of highly monodisperse silver nanoparticles from AOT reverse micelles: a way to 2D and 3D self-organization. *Chem. Mater.* **9**, 950–959 (1997).
15. Z. Nie, A. Petukhova, E. Kumacheva, Properties and emerging applications of self-assembled structures made from inorganic nanoparticles. *Nat. Nanotechnol.* **5**, 15–25 (2010).
16. N. A. Kotov, I. Dékány, J. H. Fendler, Ultrathin graphite oxide–polyelectrolyte composites prepared by self-assembly: Transition between conductive and non-conductive states. *Adv. Mater.* **8**, 637–641 (1996).
17. D. Wang, R. Kou, D. Choi, Z. Yang, Z. Nie, J. Li, L. V. Saraf, D. Hu, J. Zhang, G. L. Graff, J. Liu, M. A. Pope, I. A. Aksay, Ternary self-assembly of ordered metal oxide-graphene nanocomposites for electrochemical energy storage. *ACS Nano* **4**, 1587–1595 (2010).
18. H. B. Wu, J. S. Chen, H. H. Hng, X. W. D. Lou, Nanostructured metal oxide-based materials as advanced anodes for lithium-ion batteries. *Nanoscale* **4**, 2526–2542 (2012).
19. D. A. Dikin, S. Stankovich, E. J. Zimney, R. D. Piner, G. H. B. Dommett, G. Evmenenko, S. T. Nguyen, R. S. Ruoff, Preparation and characterization of graphene oxide paper. *Nature* **448**, 457–460 (2007).
20. I. I. Muhamad, M. H. Salehudin, E. Salleh, in *Eco-friendly polymer nanocomposites* (Springer, 2015), pp. 323–365.
21. C. Huang, X. Qiao, W. Sun, H. Chen, X. Chen, L. Zhang, T. Wang, Effective extraction of domoic acid from seafood based on postsynthetic-modified magnetic zeolite imidazolate framework-8 particles. *Anal. Chem.* **91**, 2418–2424 (2019).
22. M. Lian, Z. Xue, X. Qiao, C. Liu, S. Zhang, X. Li, C. Huang, Q. Song, W. Yang, X. Chen, T. Wang, Movable hollow nanoparticles as reactive oxygen scavengers. *Chem* **5**, 2378–2387 (2019).
23. X. Cheng, R. Sun, L. Yin, Z. Chai, H. Shi, M. Gao, Light-triggered assembly of gold nanoparticles for photothermal therapy and photoacoustic imaging of tumors in vivo. *Adv. Mater.* **29**, 1604894 (2017).
24. P. Huang, J. Lin, W. Li, P. Rong, Z. Wang, S. Wang, X. Wang, X. Sun, M. Aronova, G. Niu, R. D. Leapman, Z. Nie, X. Chen, Biodegradable gold nanovesicles with an ultrastrong plasmonic coupling effect for photoacoustic imaging and photothermal therapy. *Angew. Chem. Int. Ed. Engl.* **52**, 13958–13964 (2013).
25. L. Wang, L. Xu, H. Kuang, C. Xu, N. A. Kotov, Dynamic nanoparticle assemblies. *Acc. Chem. Res.* **45**, 1916–1926 (2012).
26. S. Ohta, D. Glancy, W. C. W. Chan, DNA-controlled dynamic colloidal nanoparticle systems for mediating cellular interaction. *Science* **351**, 841–845 (2016).
27. L. H. Tan, H. Xing, Y. Lu, DNA as a powerful tool for morphology control, spatial positioning, and dynamic assembly of nanoparticles. *Acc. Chem. Res.* **47**, 1881–1890 (2014).
28. A. Grinthal, S. H. Kang, A. K. Epstein, M. Aizenberg, M. Khan, J. Aizenberg, Steering nanofibers: An integrative approach to bio-inspired fiber fabrication and assembly. *Nano Today* **7**, 35–52 (2012).
29. M. Matsunaga, M. Aizenberg, J. Aizenberg, Controlling the stability and reversibility of micropillar assembly by surface chemistry. *J. Am. Chem. Soc.* **133**, 5545–5553 (2011).

30. T. Wang, D. LaMontagne, J. Lynch, J. Zhuang, Y. C. Cao, Colloidal superparticles from nanoparticle assembly. *Chem. Soc. Rev.* **42**, 2804–2823 (2013).
31. C. Yan, T. Wang, A new view for nanoparticle assemblies: From crystalline to binary cooperative complementarity. *Chem. Soc. Rev.* **46**, 1483–1509 (2017).
32. L. Xu, W. Ma, L. Wang, C. Xu, H. Kuang, N. A. Kotov, Nanoparticle assemblies: Dimensional transformation of nanomaterials and scalability. *Chem. Soc. Rev.* **42**, 3114–3126 (2013).
33. E. M. Sanehira, A. R. Marshall, J. A. Christians, S. P. Harvey, P. N. Ciesielski, L. M. Wheeler, P. Schulz, L. Y. Lin, M. C. Beard, J. M. Luther, Enhanced mobility $CsPbI_3$ quantum dot arrays for record-efficiency, high-voltage photovoltaic cells. *Sci. Adv.* **3**, eaao4204 (2017).
34. B. Li, K. Bian, X. Zhou, P. Lu, S. Liu, I. Brener, M. Sinclair, T. Luk, H. Schunk, L. Alarid, P. G. Clem, Z. Wang, H. Fan, Pressure compression of CdSe nanoparticles into luminescent nanowires. *Sci. Adv.* **3**, e1602916 (2017).
35. C. Liu, L. Zheng, Q. Song, Z. Xue, C. Huang, L. Liu, X. Qiao, X. Li, K. Liu, T. Wang, A metastable crystalline phase in two-dimensional metallic oxide nanoplates. *Angew. Chem. Int. Ed.* **131**, 2077–2081 (2019).
36. L. Yu, J. F. Yang, B. Y. Guan, Y. Lu, X. W. D. Lou, Hierarchical hollow nanoprisms based on ultrathin Ni-Fe layered double hydroxide nanosheets with enhanced electrocatalytic activity towards oxygen evolution. *Angew. Chem. Int. Ed. Engl.* **57**, 172–176 (2018).
37. I. Huskić, I. V. Pekov, S. V. Krivovichev, T. Friščić, Minerals with metal-organic framework structures. *Sci. Adv.* **2**, e1600621 (2016).
38. R. P. Feynman, There's plenty of room at the bottom. *Eng. Sci.* **23**, 22–36 (1960).
39. C. N. R. Rao, A. Müller, A. K. Cheetham, *The chemistry of nanomaterials: Synthesis, Properties and Applications* (John Wiley & Sons, 2006).
40. G. Schmid, *Nanoparticles: From Theory to Application* (John Wiley & Sons, 2011).
41. S. Zhao, Y. Wang, J. Dong, C.-T. He, H. Yin, P. An, K. Zhao, X. Zhang, C. Gao, L. Zhang, J. Lv, J. Wang, J. Zhang, A. M. Khattak, N. A. Khan, Z. Wei, J. Zhang, S. Liu, H. Zhao, Z. Tang, Ultrathin metal–organic framework nanosheets for electrocatalytic oxygen evolution. *Nat. Energy* **1**, 16184 (2016).
42. X. Huang, Z. Wang, Supercrystallography-based decoding of structure and driving force of nanocrystal assembly. *Materials* **12**, 3771 (2019).
43. J. Nai, B. Y. Guan, L. Yu, X. W. D. Lou, Oriented assembly of anisotropic nanoparticles into frame-like superstructures. *Sci. Adv.* **3**, e1700732 (2017).
44. D. Luo, X. Qin, Q. Song, X. Qiao, Z. Zhang, Z. Xue, C. Liu, G. Mo, T. Wang, Ordered superparticles with an enhanced photoelectric effect by sub-nanometer interparticle distance. *Adv. Funct. Mater.* **27**, 1701982 (2017).
45. X. Qiao, Z. Xue, L. Liu, K. Liu, T. Wang, Superficial-layer-enhanced raman scattering (SLERS) for depth detection of noncontact molecules. *Adv. Mater.* **31**, 1804275 (2019).
46. J. Chen, A. Dong, J. Cai, X. Ye, Y. Kang, J. M. Kikkawa, C. B. Murray, Collective dipolar interactions in self-assembled magnetic binary nanocrystal superlattice membranes. *Nano Lett.* **10**, 5103–5108 (2010).
47. M. B. Ross, J. C. Ku, V. M. Vaccarezza, G. C. Schatz, C. A. Mirkin, Nanoscale form dictates mesoscale function in plasmonic DNA–nanoparticle superlattices. *Nat. Nanotechnol.* **10**, 453–458 (2015).
48. X. Qin, D. Luo, Z. Xue, Q. Song, T. Wang, Self-assembled Ag-MXA superclusters with structure-dependent mechanical properties. *Adv. Mater.* **30**, 1706327 (2018).
49. Y. Liu, D. Luo, M. Yu, Y. Wang, S. Jin, Z. Li, S. Cui, D. He, T. Zhang, T. Wang, Thermodynamically controlled self-assembly of hierarchically staggered architecture as an osteoinductive alternative to bone autografts. *Adv. Funct. Mater.* **29**, 1806445 (2019).
50. Y. Liu, S. Liu, D. Luo, Z. Xue, X. Yang, L. Gu, Y. Zhou, T. Wang, Hierarchically staggered nanostructure of mineralized collagen as a bone-grafting scaffold. *Adv. Mater.* **28**, 8740–8748 (2016).
51. Y. Liu, D. Luo, T. Wang, Hierarchical structures of bone and bioinspired bone tissue engineering. *Small* **12**, 4611–4632 (2016).
52. L.-B. Mao, H.-L. Gao, H.-B. Yao, L. Liu, H. Cölfen, G. Liu, S.-M. Chen, S.-K. Li, Y.-X. Yan, Y.-Y. Liu, S.-H. Yu, Synthetic nacre by predesigned matrix-directed mineralization. *Science* **354**, 107–110 (2016).
53. A. O. Govorov, G. W. Bryant, W. Zhang, T. Skeini, J. Lee, N. A. Kotov, J. M. Slocik, R. R. Naik, Exciton–plasmon interaction and hybrid excitons in semiconductor–metal nanoparticle assemblies. *Nano Lett.* **6**, 984–994 (2006).
54. J. Lee, A. O. Govorov, J. Dulka, N. A. Kotov, Bioconjugates of CdTe nanowires and au nanoparticles: Plasmon–exciton interactions, luminescence enhancement, and collective effects. *Nano Lett.* **4**, 2323–2330 (2004).
55. L. Zhou, Y. Tan, J. Wang, W. Xu, Y. Yuan, W. Cai, S. Zhu, J. Zhu, 3D self-assembly of aluminium nanoparticles for plasmon-enhanced solar desalination. *Nat. Photon.* **10**, 393–398 (2016).
56. T. Wang, J. Zhuang, J. Lynch, O. Chen, Z. Wang, X. Wang, D. L. Montagne, H. Wu, Z. Wang, Y. C. Cao, Self-assembled colloidal superparticles from nanorods. *Science* **338**, 358–363 (2012).
57. M. Cargnello, A. C. Johnston-Peck, B. T. Diroll, E. Wong, B. Datta, D. Damodhar, V. V. Doan-Nguyen, A. A. Herzing, C. R. Kagan, C. B. Murray, Substitutional doping in nanocrystal superlattices. *Nature* **524**, 450–453 (2015).
58. Q. Cao, S.-j. Han, G. S. Tulevski, Y. Zhu, D. D. Lu, W. Haensch, Arrays of single-walled carbon nanotubes with full surface coverage for high-performance electronics. *Nat. Nanotechnol.* **8**, 180–186 (2013).
59. A. Dong, J. Chen, X. Ye, J. M. Kikkawa, C. B. Murray, Enhanced thermal stability and magnetic properties in NaCl-Type FePt–MnO binary nanocrystal superlattices. *J. Am. Chem. Soc.* **133**, 13296–13299 (2011).
60. S. A. Iakovenko, A. S. Trifonov, M. Giersig, A. Mamedov, D. K. Nagesha, V. V. Hanin, E. C. Soldatov, N. A. Kotov, One- and two-dimensional arrays of magnetic nanoparticles by the Langmuir–Blodgett technique. *Adv. Mater.* **11**, 388–392 (1999).
61. L. Dong, Y. Liu, Y. Lu, L. Zhang, N. Man, L. Cao, K. Ma, D. An, J. Lin, Y.-J. Xu, W.-P. Xu, W.-B. Wu, S.-H. Yu, L.-P. Wen, Tuning magnetic property and autophagic response for self-assembled Ni–Co alloy nanocrystals. *Adv. Funct. Mater.* **23**, 5930–5940 (2013).
62. O. Neumann, A. S. Urban, J. Day, S. Lal, P. Nordlander, N. J. Halas, Solar vapor generation enabled by nanoparticles. *ACS Nano* **7**, 42–49 (2012).
63. S. Gwo, H.-Y. Chen, M.-H. Lin, L. Sun, X. Li, Nanomanipulation and controlled self-assembly of metal nanoparticles and nanocrystals for plasmonics. *Chem. Soc. Rev.* **45**, 5672–5716 (2016).
64. C. Zhang, C. Yan, Z. Xue, W. Yu, Y. Xie, T. Wang, Shape-controlled synthesis of high-quality Cu_7S_4 nanocrystals for efficient light-induced water evaporation. *Small* **12**, 5320–5328 (2016).
65. H. Jin, Y. Bu, J. Li, J. Liu, X. Fen, L. Dai, J. Wang, J. Lu, S. Wang, Strong graphene 3D assemblies with high elastic recovery and hardness. *Adv. Mater.* **30**, 1707424 (2018).
66. K. Bian, Z. Wang, T. Hanrath, Comparing the structural stability of PbS nanocrystals assembled in fcc and bcc superlattice allotropes. *J. Am. Chem. Soc.* **134**, 10787–10790 (2012).
67. Z. Wang, X.-D. Wen, R. Hoffmann, J. S. Son, R. Li, C.-C. Fang, D.-M. Smilgies, T. Hyeon, Reconstructing a solid-solid phase transformation pathway in CdSe nanosheets with associated soft ligands. *Proc. Natl. Acad. Sci. U.S.A.* **107**, 17119–17124 (2010).
68. B. Su, Y. Tian, L. Jiang, Bioinspired interfaces with superwettability: From materials to chemistry. *J. Am. Chem. Soc.* **138**, 1727–1748 (2016).
69. Z. Lu, W. Zhu, X. Yu, H. Zhang, Y. Li, X. Sun, X. Wang, H. Wang, J. Wang, J. Luo, X. Lei, L. Jiang, Ultrahigh hydrogen evolution performance of under-water "superaerophobic" MoS_2 nanostructured electrodes. *Adv. Mater.* **26**, 2683–2687 (2014).
70. Q. Song, Z. Xue, C. Liu, X. Qiao, L. Liu, C. Huang, K. Liu, X. Li, Z. Lu, T. Wang, A general strategy to optimize gas evolution reaction via assembled striped-pattern superlattices. *J. Am. Chem. Soc.* **142**, 1857–1863 (2019).
71. A. E. Aliev, J. Oh, M. E. Kozlov, A. A. Kuznetsov, S. Fang, A. F. Fonseca, R. Ovalle, M. D. Lima, M. H. Haque, Y. N. Gartstein, M. Zhang, A. A. Zakhidov, R. H. Baughman, Giant-stroke, superelastic carbon nanotube aerogel muscles. *Science* **323**, 1575–1578 (2009).
72. W. H. Chong, L. K. Chin, R. L. S. Tan, H. Wang, A. Q. Liu, H. Chen, Stirring in suspension: Nanometer-sized magnetic stir bars. *Angew. Chem. Int. Ed. Engl.* **52**, 8570–8573 (2013).
73. B. Dai, J. Wang, Z. Xiong, X. Zhan, W. Dai, C.-C. Li, S.-P. Feng, J. Tang, Programmable artificial phototactic microswimmer. *Nat. Nanotechnol.* **11**, 1087–1092 (2016).
74. X. Gui, J. Wei, K. Wang, A. Cao, H. Zhu, Y. Jia, Q. Shu, D. Wu, Carbon nanotube sponges. *Adv. Mater.* **22**, 617–621 (2010).
75. K. H. Kim, Y. Oh, M. F. Islam, Graphene coating makes carbon nanotube aerogels superelastic and resistant to fatigue. *Nat. Nanotechnol.* **7**, 562–566 (2012).
76. H. Qin, T. Zhang, N. Li, H.-P. Cong, S.-H. Yu, Anisotropic and self-healing hydrogels with multi-responsive actuating capability. *Nat. Commun.* **10**, 2202 (2019).
77. L. Tian, M. Su, F. Yu, Y. Xu, X. Li, L. Li, H. Liu, W. Tan, Liquid-state quantitative SERS analyzer on self-ordered metal liquid-like plasmonic arrays. *Nat. Commun.* **9**, 3642 (2018).
78. P. Song, H. Qin, H.-L. Gao, H.-P. Cong, S.-H. Yu, Self-healing and superstretchable conductors from hierarchical nanowire assemblies. *Nat. Commun.* **9**, 2786 (2018).
79. J. Palacci, S. Sacanna, A. P. Steinberg, D. J. Pine, P. M. Chaikin, Living crystals of light-activated colloidal surfers. *Science* **339**, 936–940 (2013).
80. F. A. Lavergne, H. Wendehenne, T. Bäuerle, C. Bechinger, Group formation and cohesion of active particles with visual perception-dependent motility. *Science* **364**, 70–74 (2019).
81. X. Jiang, J. Feng, L. Huang, Y. Wu, B. Su, W. Yang, L. Mai, L. Jiang, Bioinspired 1D superparamagnetic magnetite arrays with magnetic field perception. *Adv. Mater.* **28**, 6952–6958 (2016).
82. F. Nan, F. Han, N. F. Scherer, Z. Yan, Dissipative self-assembly of anisotropic nanoparticle chains with combined electrodynamic and electrostatic interactions. *Adv. Mater.* **30**, e1803238 (2018).
83. S. Ilday, G. Makey, G. B. Akguc, Ö. Yavuz, O. Tokel, I. Pavlov, O. Gülseren, F. Ö. Ilday, Rich complex behaviour of self-assembled nanoparticles far from equilibrium. *Nat. Commun.* **8**, 14942 (2017).

84. M. E. Davis, R. J. Davis, *Fundamentals of Chemical Reaction Engineering* (Courier Corporation, 2012).
85. F. Peng, Q. Zhou, D. Zhang, C. Lu, Y. Ni, J. Kou, J. Wang, Z. Xu, Bio-inspired design: Inner-motile multifunctional ZnO/CdS heterostructures magnetically actuated artificial cilia film for photocatalytic hydrogen evolution. *Appl. Catal. B Environ.* **165**, 419–427 (2015).
86. H. Zhao, S. Sen, T. Udayabhaskararao, M. Sawczyk, K. Kučanda, D. Manna, P. K. Kundu, J.-W. Lee, P. Král, R. Klajn, Reversible trapping and reaction acceleration within dynamically self-assembling nanoflasks. *Nat. Nanotechnol.* **11**, 82–88 (2016).
87. J. Y. Park, M. J. Baek, E. S. Choi, S. Woo, J. H. Kim, T. J. Kim, J. C. Jung, K. S. Chae, Y. Chang, G. H. Lee, Paramagnetic ultrasmall gadolinium oxide nanoparticles as advanced T_1 MRI contrast agent: Account for large longitudinal relaxivity, optimal particle diameter, and *in vivo*T_1 MR images. *ACS Nano* **3**, 3663–3669 (2009).
88. S. Sharifi, S. Behzadi, S. Laurent, M. L. Forrest, P. Stroeve, M. Mahmoudi, Toxicity of nanomaterials. *Chem. Soc. Rev.* **41**, 2323–2343 (2012).
89. L. Liu, S. Chen, Z. Xue, Z. Zhang, X. Qiao, Z. Nie, D. Han, J. Wang, T. Wang, Bacterial capture efficiency in fluid bloodstream improved by bendable nanowires. *Nat. Commun.* **9**, 444 (2018).
90. H. Chen, H. Zhu, J. Hu, Y. Zhao, Q. Wang, J. Wan, Y. Yang, H. Xu, X. Yang, Highly compressed assembly of deformable nanogels into nanoscale suprastructures and their application in nanomedicine. *ACS Nano* **5**, 2671–2680 (2011).
91. G. Chen, I. Roy, C. Yang, P. N. Prasad, Nanochemistry and nanomedicine for nanoparticle-based diagnostics and therapy. *Chem. Rev.* **116**, 2826–2885 (2016).
92. T. Zhao, P. Wang, Q. Li, A. A. Al-Khalaf, W. N. Hozzein, F. Zhang, X. Li, D. Zhao, Near-infrared triggered decomposition of nanocapsules with high tumor accumulation and stimuli responsive fast elimination. *Angew. Chem. Int. Ed. Engl.* **57**, 2611–2615 (2018).
93. J. Mu, C. Hou, H. Wang, Y. Li, Q. Zhang, M. Zhu, Origami-inspired active graphene-based paper for programmable instant self-folding walking devices. *Sci. Adv.* **1**, e1500533 (2015).
94. C. Luo, C.-N. Yeh, J. M. L. Baltazar, C.-L. Tsai, J. Huang, A cut-and-paste approach to 3D graphene-oxide-based architectures. *Adv. Mater.* **30**, e1706229 (2018).
95. M. Acerce, E. K. Akdoğan, M. Chhowalla, Metallic molybdenum disulfide nanosheet-based electrochemical actuators. *Nature* **549**, 370–373 (2017).
96. C. Cheng, A. H. Ngan, Reversible electrochemical actuation of metallic nanohoneycombs induced by pseudocapacitive redox processes. *ACS Nano* **9**, 3984–3995 (2015).
97. G. Gu, M. Schmid, P.-W. Chiu, A. Minett, J. Fraysse, G.-T. Kim, S. Roth, M. Kozlov, E. Muñoz, R. H. Baughman, V_2O_5 nanofibre sheet actuators. *Nat. Mater.* **2**, 316–319 (2003).
98. T. Wang, D. Torres, F. E. Fernández, C. Wang, N. Sepúlveda, Maximizing the performance of photothermal actuators by combining smart materials with supplementary advantages. *Sci. Adv.* **3**, e1602697 (2017).
99. S. S. Agasti, S. Rana, M.-H. Park, C. K. Kim, C.-C. You, V. M. Rotello, Nanoparticles for detection and diagnosis. *Adv. drug deliver. Rev.* **62**, 316–328 (2010).
100. T. A. Taton, C. A. Mirkin, R. L. Letsinger, Scanometric DNA array detection with nanoparticle probes. *Science* **289**, 1757–1760 (2000).
101. M. Sun, L. Xu, J. H. Bahng, H. Kuang, S. Alben, N. A. Kotov, C. Xu, Intracellular localization of nanoparticle dimers by chirality reversal. *Nat. Commun.* **8**, 1847 (2017).
102. W. Ma, M. Sun, P. Fu, S. Li, L. Xu, H. Kuang, C. Xu, A chiral-nanoassemblies-enabled strategy for simultaneously profiling surface glycoprotein and MicroRNA in living cells. *Adv. Mater.* **29**, 1703410 (2017).
103. J. Kumar, H. Eraña, E. López-Martínez, N. Claes, V. F. Martín, D. M. Solís, S. Bals, A. L. Cortajarena, J. Castilla, L. M. Liz-Marzán, Detection of amyloid fibrils in Parkinson's disease using plasmonic chirality. *Proc. Natl. Acad. Sci. U.S.A.* **115**, 3225–3230 (2018).
104. C. J. Danby, J. G. Davoud, D. H. Everett, C. N. Hinshelwood, R. M. Lodge, 202. The kinetics of absorption of gases from an air stream by granular reagents. *J. Chem. Soc.* **115**, 918–934 (1946).
105. L. A. Jonas, J. A. Rehrmann, Predictive equations in gas adsorption kinetics. *Carbon* **11**, 59–64 (1973).
106. Y. Wang, X. Peng, A. Abelson, P. Xiao, C. Qian, L. Yu, C. Ophus, P. Ercius, L.-W. Wang, M. Law, H. Zheng, Dynamic deformability of individual PbSe nanocrystals during superlattice phase transitions. *Sci. Adv.* **5**, eaaw5623 (2019).
107. X. Huang, J. Zhu, B. Ge, K. Deng, X. Wu, T. Xiao, T. Jiang, Z. Quan, Y. C. Cao, Z. Wang, Understanding Fe_3O_4 nanocube assembly with reconstruction of a consistent superlattice phase diagram. *J. Am. Chem. Soc.* **141**, 3198–3206 (2019).
108. Y. Xia, Y. Xiong, B. Lim, S. E. Skrabalak, Shape-controlled synthesis of metal nanocrystals: Simple chemistry meets complex physics? *Angew. Chem. Int. Ed. Engl.* **48**, 60–103 (2009).
109. B. O. Dabbousi, J. Rodriguez-Viejo, F. V. Mikulec, J. R. Heine, H. Mattoussi, R. Ober, K. F. Jensen, M. G. Bawendi, (CdSe)ZnS core-shell quantum dots: Synthesis and characterization of a size series of highly luminescent nanocrystallites. *J. Phys. Chem. B* **101**, 9463–9475 (1997).
110. A. Banerjee, D. Bernoulli, H. Zhang, M.-F. Yuen, J. Liu, J. Dong, F. Ding, J. Lu, M. Dao, W. Zhang, Y. Lu, S. Suresh, Ultralarge elastic deformation of nanoscale diamond. *Science* **360**, 300–302 (2018).

Acknowledgments

Funding: This work was financially supported by the National Natural Science Foundation of China (21925405, 21635002, and 201874005), the National Key Research and Development Program of China grant no. 2018YFA0208800, and the Chinese Academy of Sciences (XDA23030106 and YJKYYQ20180044). **Author contributions:** T.W. conceived the ideas and planned the content. C.H. wrote the first draft. All authors worked on the final draft. **Competing interests:** The authors declare that they have no competing interests. **Data and materials availability:** All data needed to evaluate the conclusions in the paper are present in the paper and/or the materials cited herein. Additional data related to this paper may be requested from the authors.

Submitted 7 November 2019
Accepted 27 February 2020
Published 13 May 2020
10.1126/sciadv.aba1321

Citation: C. Huang, X. Chen, Z. Xue, T. Wang, Effect of structure: A new insight into nanoparticle assemblies from inanimate to animate. *Sci. Adv.* **6**, eaba1321 (2020).